# Noise-Induced Current Switching in Semiconductor Superlattices: Observation of Nonexponential Kinetics in a High-Dimensional System

Yu. Bomze, R. Hey, H. T. Grahn, and S. W. Teitsworth

Phys. Rev. Lett. **109**, 026801 — Published 9 July 2012

DOI: 10.1103/PhysRevLett.109.026801

# Noise-Induced Current Switching in Semiconductor Superlattices: Observation of Non-Exponential Kinetics in a High-Dimensional System

Yu. Bomze,[1] R. Hey,[2] H. T. Grahn,[2] and S. W. Teitsworth[1]

[1] *Duke University, Department of Physics, Box 90305, Durham, NC 27708-0305*
[2] *Paul-Drude-Institut für Festkörperelektronik, Hausvogteiplatz 5–7, 10117 Berlin, Germany*

(Dated: June 13, 2012)

We report on measurements of first-passage-time distributions associated with current switching in weakly coupled GaAs/AlAs superlattices driven by shot noise, a system that is both far-from-equilibrium and high-dimensional. Static current-voltage ($I$-$V$) characteristics exhibit multiple current branches and bistability; precision, high-bandwidth current switching data are collected in response to steps in the applied voltage to final voltages $V_1$ near the end of a current branch. For a range of $V_1$ values, the measured switching times vary stochastically. At short times ($\lesssim 10$ $\mu$s), the switching time distributions decay exponentially, while at longer times the distributions develop non-exponential tails that follow an approximate power law over several decades. The power law decay behavior is attributed to the presence of multiple switching pathways, which may arise from small spatial variations in the superlattice growth parameters.

PACS numbers: 05.40.-a, 05.10.Gg, 73.50.Fq, 73.21.Cd

The phenomenon of noise-driven escape from a metastable state plays an important role in a wide range of natural systems, such as chemical reactions [1], switching between bistable vibrational states in nano- and micro-mechanical oscillators [2–4], magnetization switching in ferromagnetic nanoparticles [5] and submicron thin films [6, 7], spin torque switching in magnetic tunnel junctions [8], switching in genetic regulatory networks [9], and switching between dynamic, current-carrying states in a variety of electronic transport systems including driven Josephson junctions [10, 11], resonant tunneling structures [12], and semiconductor superlattices [13–15]. These systems fall into two broad categories: those that are near-equilibrium (e.g., chemical reactions and magnetization switching) and those that are far-from-equilibrium (e.g., driven Josephson junctions, resonant tunneling systems, and driven mechanical oscillators). One central feature that is addressed in both theoretical and experimental work is the first-passage-time distribution (FPTD), i.e., the distribution of times when identically prepared systems first escape the metastable state. For a general dynamical system with escape occurring via a single saddle point, the FPTD is expected to show an exponential tail at long times [16]. Furthermore, it is important to study how the mean switching time and FPTD evolve with a control parameter in the neighborhood of the bifurcation in which the metastable state disappears [12, 17–19]. However, there have been only a few reported experimental studies of the FPTD for high-dimensional, far-from-equilibrium systems [13, 14, 20].

Here we describe the measurement of FPTDs associated with the transition from a metastable state of the electrical current in a doped, weakly coupled GaAs/AlAs semiconductor superlattice (SL). A semiconductor SL with $N \gg 1$ periods constitutes a high-dimensional, far-from-equilibrium system. Furthermore, the system cannot be described as the gradient of an effective potential energy function, a property that follows from standard models of SL electronic transport in which the $N$ dynamical variables correspond to the spatial averages of electric field over each SL period [21, 22]. Under sufficiently large voltage bias, the SL exhibits the formation of static electric-field domains: a region of low electric field next to the emitter contact, followed by a charge accumulation layer (CAL) localized in one quantum well, and then a region of high electric field next to the collector contact. This behavior manifests itself in measured current-voltage ($I$-$V$) characteristics that possess several current branches, where each branch corresponds to the location of the CAL in a particular quantum well and where the total number of branches is approximately equal to the number of periods $N$. Figure 1(a) shows a single hysteretic current loop associated with the transition between the $13^{\text{th}}$ and $14^{\text{th}}$ branch; the inset shows the $I$-$V$ characteristic over the full voltage range studied. Figures 1(b) and 1(c) show the spatial distribution of electric-field domains corresponding to the $13^{\text{th}}$ and $14^{\text{th}}$ branch, respectively. With increasing applied voltage, as the current jumps from one branch to the next, the CAL moves by one well toward the emitter.

In this paper, current switching statistics are studied as a function of the applied voltage $V_1$ in the neighborhood of the transition voltage $V_{\text{th}}$, defined as the voltage for which the measured $I$-$V$ curve jumps from one branch to the next as the applied voltage increases [$V_{\text{th}} = 2.384$ V in Fig. 1(a)]. As such, $V_{\text{th}}$ constitutes a lower bounding approximation to the voltage where the upper current branch is predicted to end in a saddle-node bifurcation [21]. We measure switching statistics with an exceptionally large dynamic range, measured over approximately *nine* decades of time. This is much larger than achieved in previous studies of current switching in

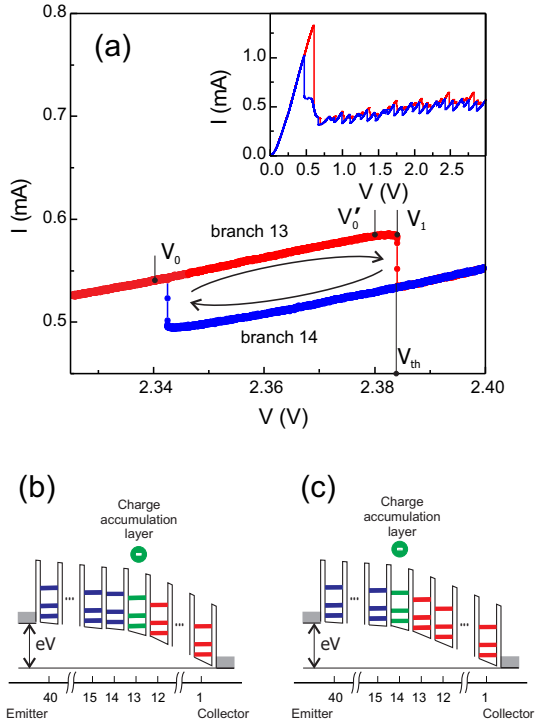


FIG. 1. (a) Hysteretic $I$-$V$ loop associated with the coexisting $13^{\text{th}}$ and $14^{\text{th}}$ current branches. Inset: Measured $I$-$V$ characteristic over a larger voltage range. Corresponding electric-field domain profiles and charge accumulation layer locations for (b) the $13^{\text{th}}$ and (c) the $14^{\text{th}}$ branch.

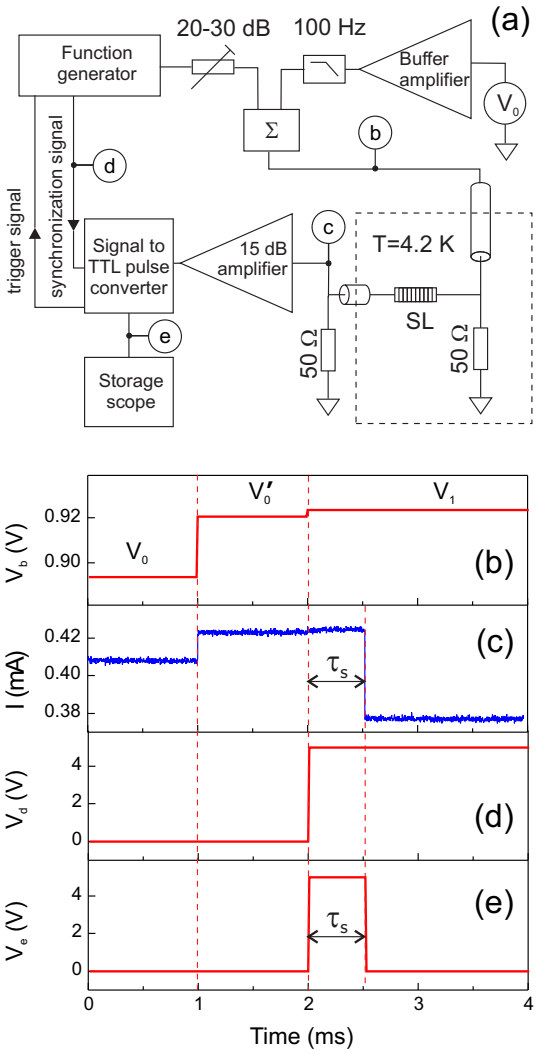


FIG. 2. (a) Experimental schematic for measuring stochastically varying switching times between different current states at 4.2 K. (b) Applied voltage signal to the SL at point labeled ⓑ for the transition from the $2^{\text{nd}}$ to the $3^{\text{rd}}$ branch. (c) Time-dependent current response through the SL measured at point ⓒ. (d) Synchronization signal from AFG to Transistor-Transistor-Logic (TTL) level pulse converter, cf. point ⓓ. (e) Output of TTL pulse converter, which provides the measured switching times $\tau_s$, cf. point ⓔ.

SLs [13, 14] and is enabled by using a novel measurement approach. In addition to observing an exponential decay of the switching time distributions for $V_1$ near to $V_{th}$, we observe long-time tails with an approximate power law form, which become more prominent as the mean metastable state lifetime increases.

The investigated sample consists of a 40-period SL with 9-nm-wide GaAs wells and 4-nm-wide AlAs barriers grown by molecular beam epitaxy on a doped GaAs substrate. The central 5 nm of each well are Si doped with a density of $3\times10^{17}$ cm$^{-3}$. The SL is sandwiched between GaAs contact layers with graded doping that ranges from nominally zero (next to the first AlAs barrier) to $3\times10^{18}$ cm$^{-3}$ over a distance of 100 nm. The sample is supplied with Ohmic Au-Ni-Ge contacts and chemically etched into several mesas with diameters of 120 and 200 $\mu$m. All data displayed in this paper are for a single 200 $\mu$m mesa. Data collected for other mesas with the same and smaller diameter are similar. The sample is mounted on a custom-built, gold-plated, copper-clad printed-circuit board, which is immersed in liquid helium and connected to room temperature equipment via low-noise, high-frequency coaxial cables (3 dB attenuation at 1 GHz for the used length) with micro coaxial connectors. All measurements were performed at 4.2 K.

The experimental schematic for measuring switching times is shown in Fig. 2(a). A novel feature of the approach, not used in previous measurements of first-passage distributions [3, 6, 8, 13, 14, 20, 24], is the implementation of a self-triggering protocol (described below), which allows for the measurement of switching times over an exceptionally large dynamic range, in this case, approximately $10^9$, ranging from about 4 ns to 10 s. The starting applied voltage $V_0$ is selected to lie on a monostable part of the $I$-$V$ curve [cf. Fig. 1(a)]; the system is held at this voltage for 1 ms to insure that transients decay. Then, the voltage is stepped to $V_0'$, which is closer to the transition voltage $V_{\text{th}}$, but sufficiently below it so

that noise-induced switching to the next current branch does not occur. The system is held at $V_0'$ for 1 ms. Finally, the voltage is stepped to a value $V_1$ for which the system exhibits noise-induced switching to the next current branch.

To form the complete voltage signal, we use a constant voltage $V_0$ produced by a low-noise voltage reference buffered with a power amplifier and a 100 Hz low-pass filter. We add to this voltage steps produced by an arbitrary function generator (AFG) [Tektronix AFG3252] to reach the levels $V_0'$ and $V_1$. Since the AFG is the main source of external noise in this experiment, we use its full 5 V output range followed by an attenuation of 26 dB to increment the applied voltage at the sample in steps as small as 30 $\mu$V with a noise level of 50 $\mu$V rms, about one order of magnitude smaller than voltage fluctuations due to internal shot noise of the SL, estimated as $r\sqrt{eI\Delta f} \sim 300$ $\mu$V rms, where $r \sim 1$ k$\Omega$ and $\Delta f \sim 1$ GHz denote SL differential resistance and bandwidth, respectively. The AFG and voltage reference outputs are added together using a passive power combiner [point ⓑ in Fig. 2(a)], and the resultant voltage signal shown in Fig. 2(b) is applied to the sample through 50 $\Omega$ matched low-noise, high-frequency coaxial cables. The SL current response is detected as a voltage drop through the 50 $\Omega$ non-inverting input of a low-noise, wide-bandwidth (3 GHz) amplifier [cf. point ⓒ in Fig. 2(a)]. After the applied voltage reaches $V_1$, the SL current undergoes a transition to the lower branch with a stochastically varying switching time $\tau_s$ as shown in Fig. 2(c).

In order to measure the switching time statistics over a wide dynamic range, we use a *self-triggering* protocol: 1) the AFG outputs a 5 Volt (TTL level) signal synchronized with the $V_1$ voltage step, which is supplied to a signal-to-TTL pulse converter [cf. point ⓓ in Fig. 2(a)]; 2) the sample current response and synchronization signal are combined to form a 5 Volt pulse with a width equal to the switching time $\tau_s$ [shown in Fig. 2(e)]; 3) the trailing edge of the constructed pulse triggers the AFG in order to initiate a new $V_0 \rightarrow V_0' \rightarrow V_1$ control signal; and 4) a high-bandwidth digital oscilloscope (DPO) [Tektronix DPO7104] is triggered by both leading and trailing edges in order to extract individual $\tau_s$ values with a timing accuracy of 4 ns or 2 ppm, whichever is larger. This allows for the measurement of $\tau_s$ values that are several orders of magnitude larger than the DPO sampling time of 1 ns. Note also that $\tau_s$ is defined as the time when the current first reaches the midpoint between the upper and the lower branch. The results described below are essentially independent of the current detection point, which can be set at any value, provided it is not too close to either the upper or lower branch current level, i.e., closer than 5 $\mu$A for this experiment. Furthermore, simulations indicate that, for voltages for which stochastic switching is observable, the current difference between the metastable and saddle point state is much less than 5 $\mu$A [21, 26]; for this reason, the experimental detection point always lies between the saddle point state and final (i.e., initially empty) stable state and is well-separated from either of these two states. We record up to $10^5$ switching events for each value of $V_1$.

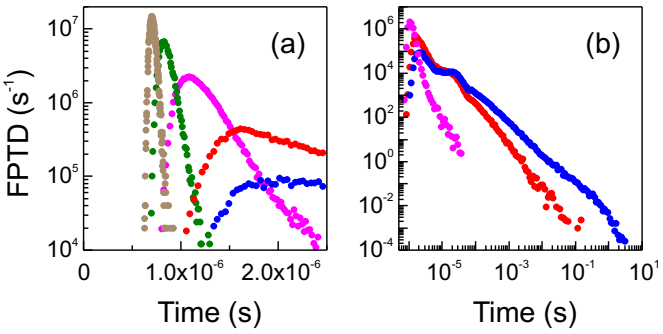


FIG. 3. Switching time distributions for transitions from the 13$^{\text{th}}$ to the 14$^{\text{th}}$ current branch: (a) at shorter times in a log-linear representation and (b) at longer times in a log-log representation. The different colors correspond to the following voltage values: $v = 1.0$ mV (brown), 700 $\mu$V (green), 400 $\mu$V (magenta), 175 $\mu$V (red), and 50 $\mu$V (blue).

Representative switching time distributions are shown for different values of applied voltage $v \equiv V_1 - V_{\text{th}}$ in Fig. 3. For applied voltages well above the transition, i.e., $v \gtrsim 3$ mV, the system undergoes a nearly deterministic transition to the stable current state, and the distribution has a Gaussian form [cf. the brown curve in Fig. 3(a)] which is narrowly distributed about a mean time of about 0.5 $\mu$s. For 300 $\mu$V$\lesssim v \lesssim 3$ mV, the distribution becomes asymmetric with a long-time exponential tail and a characteristic decay time that increases with decreasing $v$ [cf. the green and magenta curves in Fig. 3(a)]. For $v \lesssim 300$ $\mu$V, the distribution develops an approximate power law decay over several decades of time with distinct inflection features [cf. the red and blue curves in Fig. 3(b)]. The power law decay is of the form $t^{-\alpha}$ with $\alpha$ varying from 2 to 1 as the applied voltage decreases. For the red curve of Fig. 3(b), we have $\alpha = 1.97$, and for the blue curve $\alpha = 1.35$. To quantify the dependence of the switching time distributions on the applied voltage, we compute mean and median times and extract exponential decay times from the intermediate time behavior; these are plotted vs. $v$ in Fig. 4(a). We observe that all three times increase exponentially with decreasing $v$ near $v \approx 0$, in qualitative agreement with theoretical expectations. Since $V_{\text{th}}$ is only a lower bounding approximation to the true bifurcation voltage, $v$ is not the same as the distance to the bifurcation point. For this reason, it is not possible to extract a scaling relationship between mean time and distance to the bifurcation point, which could be quantitatively compared with theory [12, 17–19, 25]. Figure 4(b) shows the mean time $\tau$ vs. the ratio of the median to the mean time $\tau_m/\tau$. For a Gaussian distribu-

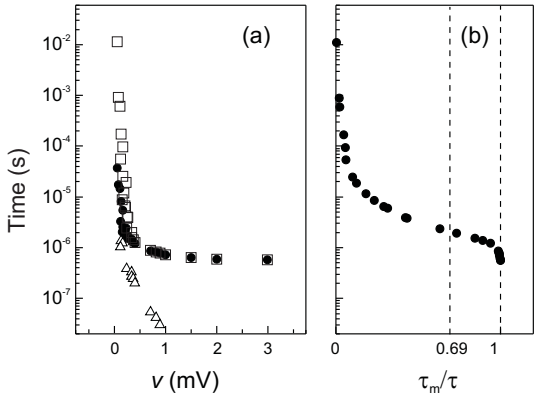


FIG. 4. (a) Characteristic times versus applied voltage $v$: exponential slope times (open triangles), mean times (open squares), and median times (closed circles). (b) Mean time $\tau$ vs. ratio of the median to the mean time (i.e., $\tau_m/\tau$), showing the transition in the form of the distributions from Gaussian to long tail, quasi-power law form.

tion, we have $\tau_m/\tau = 1$, for a simple exponential decay $\tau_m/\tau = 0.69$, while for a power law decay $\tau_m/\tau$ depends on the power law exponent and tends to 0 for a power law decay slower than $1/t^2$. Figure 4(b) shows that the distribution evolves from a Gaussian to a quasi-power law form as $\tau$ ranges from $10^{-6}$ to $10^{-5}$ s.

While the mean time data of Fig. 4 are qualitatively consistent with theoretical predictions, the presence of long-time tails in the underlying distributions, cf. Fig. 3 is not expected. For escape from a metastable to a globally stable state via a single saddle point, theory predicts a switching time distribution that is exponential at long times, see, e.g., Ref. [16]. The presence of power law tails in the measured distributions suggests the presence of multiple escape pathways. In actual SLs, such multiple pathways could arise from small spatial variations in the growth parameters. For example, in the vertical direction (i.e., parallel to current flow), each quantum well has slightly different doping levels; in theoretical work, this has been shown to produce a large set of secondary metastable states that are close to the primary metastable state [27]. In the lateral direction (i.e., parallel to the SL heterointerfaces), monolayer variations in well and barrier thicknesses will give rise to one or more preferred regions for the switching process to initiate [12]. In principle, secondary metastable states might be observable in current-time traces as multiple, distinct current levels prior to switching. In this experiment, we have not observed such behavior which implies that, if secondary metastable states are present, the associated current differences are significantly less than 5 $\mu$A.

We have presented a novel technique for measuring noise-driven current switching statistics from a metastable to a globally stable state in a semiconductor superlattice. This approach is generally well-suited to measure distributions that span several decades in time, and it is applicable to a wide range of systems [3, 6, 8, 14, 20, 24]. For relatively small values of the mean switching time near the end of a current branch, the measured distributions possess simple exponential tails. However, for larger mean switching times, long-time tails with an approximate power law form are observed. Thus, the probability to observe switching events at very long times is orders of magnitude larger than expected for an exponential decay.

We acknowledge helpful discussions with Matthew Hastings and Kostantin Matveev. This work was supported by the National Science Foundation through grant DMR-08-04232.

[1] P. Hänggi, P. Talkner, and M. Borkovec, Rev. Mod. Phys. **62**, 251 (1990).

[2] J. S. Aldridge and A. N. Cleland, Phys. Rev. Lett. **94**, 156403 (2005).

[3] H. B. Chan and C. Stambaugh, Phys. Rev. Lett. **99**, 060601 (2007).

[4] H. B. Chan, M. I. Dykman, and C. Stambaugh, Phys. Rev. Lett. **100**, 130602 (2008).

[5] W. Wernsdorfer *et al.*, Phys. Rev. Lett. **78**, 1791 (1997).

[6] R. H. Koch *et al.*, Phys. Rev. Lett. **84**, 5419 (2000).

[7] G. Grinstein and R. H. Koch, Phys. Rev. B **71**, 184427 (2005).

[8] Y.-T. Cui *et al.*, Phys. Rev. Lett. **104**, 097201 (2010).

[9] E. Aurell and K. Sneppen, Phys. Rev. Lett. **88**, 048101 (2002).

[10] M. H. Devoret, D. Esteve, J. M. Martinis, A. Cleland, and J. Clarke, Phys. Rev. B **36**, 58 (1987).

[11] D. Vion, M. Götz, P. Joyez, D. Esteve, and M. H. Devoret, Phys. Rev. Lett. **77**, 3435 (1996).

[12] O. A. Tretiakov, T. Gramespacher, and K. A. Matveev, Phys. Rev. B **67**, 073303 (2003).

[13] K. J. Luo, H. T. Grahn, and K. H. Ploog, Phys. Rev. B **57**, R6838 (1998).

[14] M. Rogozia, S. W. Teitsworth, H. T. Grahn, and K. H. Ploog, Phys. Rev. B **64**, 041308 (2001).

[15] L. L. Bonilla, O. Sánchez, and J. Soler, Phys. Rev. B **65**, 195308 (2002).

[16] N. G. van Kampen, *Stochastic Processes in Physics and Chemistry*, 3rd ed. (Elsevier, Amsterdam, 2007).

[17] J. Kurkijärvi, Phys. Rev. B **6**, 832 (1972).

[18] R. H. Victora, Phys. Rev. Lett. **63**, 457 (1989).

[19] M. I. Dykman, E. Mori, J. Ross, and P. M. Hunt, J. Chem. Phys. **100**, 5735 (1994).

[20] A. R. Hall, J. M. Keegstra, M. C. Duch, M. C. Hersam, and C. Dekker, Nano Lett. **11**, 2446 (2011).

[21] L. L. Bonilla and H. T. Grahn, Rep. Prog. Phys **68**, 577 (2005).

[22] L. L. Bonilla and S. W. Teitsworth, *Nonlinear Wave Methods for Charge Transport* (Wiley-VCH, Berlin, 2010).

[23] P. Rodin and E. Schöll, Phys. Rev. B **71**, 047301 (2005).

[24] M. Wiggin, C. Tropini, V. Tabard-Cossa, N. N. Jetha, and A. Marziali, Biophys. J. **95**, 5317 (2008).

[25] M. Heymann, S. W. Teitsworth, and J. Mattingly, arXiv 1008.4037 (2010).

[26] Huidong Xu, Ph. D. thesis, Duke University (2010).

[27] M. Patra, G. Schwarz, and E. Schöll, Phys. Rev. B **57**, 1824 (1998).